Somatostatin interneurons in auditory cortex regulate cortical representations and contribute to auditory perception

Ruiming Chai[1,2], Yuan Zhang[1], Yu Xin[1], Li Deng[1], and Ning-long Xu[1,2,3]*

[1] Institute of Neuroscience, State Key Laboratory of Neuroscience, CAS Center for Excellence in Brain Science and Intelligence Technology, Chinese Academy of Sciences, Shanghai 200031, China.

[2] University of Chinese Academy of Sciences, Beijing 100049, China.

[3] Shanghai Center for Brain Science and Brain-Inspired Intelligence Technology, Shanghai 201210, China.

Correspondence: Ning-long Xu, xunl@ion.ac.cn

Abstract

As a major class of inhibitory neurons in the mammalian neocortex, somatostatin (SOM)-expressing GABAergic interneurons receive diverse inputs and target multiple types of local cortical neurons, representing a critical circuit component. Yet, the precise contribution of SOM interneurons to cortical circuit function and behavioral performance remains unclear. Here we address this using cell-type specific imaging and perturbation during an auditory perceptual decision task. Two-photon calcium imaging reveals that SOM interneurons exhibit task enhanced responses and stimulus category selectivity. Simultaneous optogenetic inactivation and two-photon imaging show that SOM interneurons exert divergent effects of either sharpening the sensory tuning or scaling down the tuning peak on different proportions of auditory cortical neurons. At behavioral level, inactivation of SOM interneurons reveals a specific contribution to perceptual discriminability. Our data delineate the role of SOM interneurons in cortical processing and auditory perception, linking cell-type specific cortical circuit computations with perceptual functions.

Introduction

Cortical inhibitory interneurons comprise diverse classes, forming distinct circuit motifs and exhibiting various functional properties (Fishell and Rudy, 2011; Kepecs and Fishell, 2014; Markram et al., 2004; Tremblay et al., 2016). Three genetically distinct subtypes of GABAergic interneurons expressing, parvalbumin (PV), vasointestinal peptide (VIP) and somatostatin (SOM), respectively, constitute the majority of cortical inhibitory interneurons. The molecular, anatomical and physiological properties of these different subtypes of interneurons have been intensively studied in the past decades. However, it was not until recently that the impact of specific subtypes of interneurons on cortical circuit processing and behavioral functions began to be unraveled (Kepecs and Fishell, 2014).

While considerable progresses have been made in understanding the circuitry and behavioral functions of PV interneurons (Iaccarino et al., 2016; Lee et al., 2012; Letzkus et al., 2011; Schneider et al., 2014; Sohal et al., 2009; Yizhar et al., 2011) and VIP interneurons (Fu et al., 2014; Lee et al., 2013; Letzkus et al., 2011; Pi et al., 2013), it is much less clear regarding the functions of SOM interneurons (Urban-Ciecko and Barth, 2016). As a major class of GABAergic interneurons in the cortex, SOM interneurons possess unique functional properties. They target dendrites of pyramidal neurons (Chiu et al., 2013; Muñoz et al., 2017; Murayama et al., 2009; Silberberg and Markram, 2007), and provide powerful inhibition to other types of GABAergic interneurons as well as to local excitatory neurons (Cottam et al., 2013; Pfeffer et al., 2013). SOM interneurons also receive top-down feedback (Liu et al., 2020) and neuromodulatory inputs (Chen et al., 2015), and are modulated by sensory experience, behavioral state and learning (Kato et al., 2015; Khan et al., 2018; Kuchibhotla et al., 2017; Pakan et al., 2016). Like PV interneurons, SOM interneurons also contribute to cortical rhythmic activity (Chen et al., 2017; Veit et al., 2017). Despite these functional implications, it is yet to be determined how SOM interneurons regulate cortical circuit computations in relation to precisely defined behavioral events (Kepecs and Fishell, 2014). It has been debated whether SOM interneurons exert a subtractive or divisive effect on sensory tuning properties when being experimentally activated in sensory cortex (Atallah et al., 2012, 2014; El-Boustani; El-Boustani and Sur, 2014; Lee; Lee et al., 2012; Phillips and Hasenstaub, 2016; Wilson et al., 2012). While a potential reconcile was made by proposing that network

configuration changes could account for the mixed observations of SOM neurons' inhibitory roles (Seybold et al., 2015), the mechanisms could be more complex given the diverse targets of SOM neurons, including both excitatory and inhibitory neurons as well as different subcellular compartments of pyramidal neurons. Moreover, previous studies examining the effect of SOM interneurons on local circuit functions mostly used optogenetic activation (Atallah et al., 2012; El-Boustani and Sur, 2014; Lee et al., 2012; Seybold et al., 2015; Wilson et al., 2012), but inactivation experiments under well controlled behavior are scarcely done, which are essential to reveal the more physiological and causal contributions of SOM interneurons to cortical circuits and behavioral functions.

To elucidate how cortical SOM interneurons influence local circuit processing and contribute to perceptual behavior, we use cell-type specific *in vivo* two-photon imaging to record SOM interneuron activity in mouse auditory cortex during a psychophysics task measuring auditory perception and decision-making, and used optogenetic and chemogenetic inactivation to probe the causal role of SOM interneurons in cortical circuits and perceptual functions. We found that SOM interneurons show selective responses to sensory stimuli and encode task variables. The response magnitude was markedly modulated by task performance, suggesting the participation of SOM interneurons in auditory perception. Chronic imaging from the same population of SOM interneurons across days over task training showed that the behavior-related modulation emerged over learning. Furthermore, using simultaneous optogenetic inactivation and two-photon imaging, we found that SOM interneurons exert both sharpening and scaling effects on the frequency tuning of different subpopulations of local cortical neurons during auditory discrimination task. Consistent with the greater sensory sharpening effect, inactivation of SOM interneurons significantly reduced perceptual sensitivity during perceptual discrimination. These results reveal the critical role of SOM interneuron in cortical circuit computation and its contribution to auditory percep tion.

Results

We trained head-fixed mice to perform an auditory-guided perceptual decision task (Xin et

al., 2019; Zhong et al., 2019), discriminating various tone frequencies as lower or higher than a predefined category boundary, and reporting their decisions by licking the left or right water spout (**Figure 1A**). To image the activity of SOM interneurons, we expressed genetically encoded calcium sensor GCaMP6s in a Cre-dependent manner by injecting AAV-Syn-FLEX-GCaMP6s to unilateral auditory cortex of SOM-Cre mice, and implanted a chronic imaging window above the injection site. Using *in vivo* two-photon microscopy with a tiltable objective we imaged the auditory cortex when mice were performing the head-fixed auditory decision-making task (**Figure 1B**). We imaged 846 SOM interneurons from layer 2/3 (L2/3) of mouse auditory cortex during task performance, and observed large evoked calcium transients in SOM interneurons during task performance (**Figures 1B** and **1C**). SOM interneurons showed diverse response patterns, either selective to tone frequencies or to categorical choices (**Figure 1D**).

To understand how SOM interneurons participate in perceptual behavior, we first compared their activity between task performance state and passive listening state. We recorded the activity of SOM interneurons outside of task performance (passive listening state) by delivering the same set of tone stimuli after mice finished each behavioral session and were quietly awake. We found that many SOM interneurons exhibited differential responses between the task performance condition and the passive listening condition (**Figure 1D**). Overall, task performance significantly enhanced the response amplitude of SOM interneurons (**Figure 1E**). To compare the task relevant information coding of SOM interneurons between task and passive states, we computed the area under the receiver operating characteristic curve (auROC, **Methods**) to indicate individual neurons' discriminability of choice-related stimulus category. We found that the capability of discriminating stimulus categories by individual SOM interneurons was also significantly enhanced during task performance (**Figure 1F** and **S1**). These results suggest that SOM interneurons may exert enhanced regulation on local cortical circuits during perceptual discrimination task.

It was previously shown that SOM interneuron activity was modulated by learning (Kato et al., 2015; Khan et al., 2018). We thus examined whether the task-related enhancement in

SOM interneuron function may arise from learning. We performed chronic imaging to track the activity of 88 SOM interneurons in the auditory cortex across task learning (**Figures 2A** and **2B**), first in early learning stage (correct rate < 60%) then in expert stage (correct rate > 80%). As shown in **Figures 2C** and **2D**, in early task training stage a SOM interneuron showed similar responses to tone stimuli between task and passive conditions (**Figure 2C**). But during expert stage, the same SOM interneuron showed enhanced responses to tone stimuli of the low frequency category during task performance comparing to responses during passive stimulation (**Figure 2D**). Over the population, SOM interneuron responses were not significantly different between task and passive conditions in early learning stage (**Figure 2E**), whereas the responses of the same group of SOM interneurons were significantly enhanced by task performance in expert stage (**Figure 2F**). We also examined the changes in task relevant information coding of SOM interneurons over learning. During early learning stage, the capability of discriminating stimulus categories by individual SOM interneurons was not significantly different between task and passive conditions (**Figure 2G**). However, such neuronal discrimination of stimulus categories was significantly higher during task performance than during passive listening in expert stage (**Figure 2H**), consistent with our observation in well-trained mice (**Figure 1F**). In the meanwhile, the basic frequency preferences of individual neurons appear to be largely unchanged over learning (**Figure S2**). These data suggest that the task-related enhancement of responses and categorization-related information coding in SOM interneurons emerged over learning.

To investigate the role of SOM neurons in regulating cortical circuit computations during perceptual discrimination behavior, we employed simultaneous *in vivo* two-photon imaging and optogenetics to record local population activity while inactivating SOM interneurons during task performance (**Figure 3A**). We injected a mixture of AAV-hSyn-FLEX-Jaws-tdTomato and AAV-hSyn-GCaMP6s to the auditory cortex of SOM-Cre mice to express Jaws (a red light activated activity suppressor) in SOM interneurons and GCaMP6s in the L2/3 neurons (**Figure 3A**). Photostimulation strongly inhibited the responses of Jaws expressing SOM interneurons (**Figure S3**), while led to a general increase in the responses of local cortical neurons (**Figures 3B** and **3C**), indicating a general inhibitory effect of SOM

interneurons on the L2/3 population.

Besides the general inhibitory effect, SOM interneurons may exert more specific effects on local circuit processing. To further examine this, we compared single neuron responses during task performance with or without photoinhibition of SOM interneurons. To understand the potential contributions to sensory discrimination, we focused on the neurons with selectivity to tone frequency instead of those with selectivity to choices (**Methods; Figure S4**). We found that photoinhibition of SOM interneurons led to structured changes in the response properties of local neurons. In one type of neurons (type I), photoinhibition of SOM interneurons led to stronger enhancement of responses to non-preferred stimuli than to preferred stimuli, resulting in broadened tuning width (**Figures 3D** and **3F**). This suggests that SOM interneuron activity normally sharpens the frequency tuning of these neurons. In another type of neurons (type II), photoinhibition of SOM interneurons preferentially increased the responses to the preferred frequency, suggesting a scaling effect on stimulus tuning by SOM interneuron activity (**Figures 3E, 3G** and **3H**).

The sharpening of frequency tuning (type I) is likely to increase neuronal stimulus discriminability, while the scaling of the tuning curve (type II) is likely to have an effect on stimulus detection. Since our current task is a frequency discrimination task with the stimulus intensity well above detection threshold (Xin et al., 2019) (**Methods**), the behavioral performance primarily depends on stimulus discrimination rather than stimulus detection. We thus examined the contribution of SOM interneurons to stimulus discriminability by individual neurons of these two modulation types. As expected, we found that for type I neurons, photoinhibition of SOM interneurons significantly reduced neuronal discrimination of stimulus pairs with smaller frequency differences (**Figure 3I**), suggesting that SOM interneurons contribute to the fine discrimination of tones by these neurons. For type II neurons, photoinhibition of SOM interneurons did not significantly change their discriminability of stimulus pairs (**Figure 3J**). Overall, there are greater proportion of type I neurons (23%) showing sharpening of frequency tuning by SOM interneurons than type II neurons (9%) showing scaling of tuning by SOM interneurons during the behavioral task (**Figure 3K**).

To further examine the contribution of SOM interneurons to perception-level frequency discrimination, we reversibly silenced SOM interneurons of the auditory cortex in both hemispheres during task performance using chemogenetics. We expressed hM4Di in SOM interneurons in auditory cortex by bilateral injection of AAV-hSyn-FLEX-hM4Di-mCherry in SOM-Cre mice (**Figure 4A**). Clozapine-N-oxide (CNO) or saline (as control) was administered via intraperitoneal (IP) injection prior to each behavioral session on alternating days. We found that inactivation of SOM interneurons in the auditory cortex significantly impaired behavioral performance of auditory discrimination as indicated by reduced slope of psychometric functions following CNO injection comparing to saline injection (**Figures 4B** and **4C**). Consistent with the reduction in psychometric slopes, we found that inactivation of SOM interneurons significantly reduced task performance on more difficult trials with frequencies closer to the category boundary (**Figure 4D**), but not for performance on easy trials (with frequencies on the two ends of tested frequency range) (**Figure 4E**), indicating that the activity of SOM interneurons contributed to finer perceptual discrimination. To control for the possible non-specific effect of CNO injection, we expressed tdTomato in SOM interneurons of auditory cortex by bilateral injection of AAV-hSyn-FLEX-tdTomato in SOM-Cre mice (**Figure 4F**), and found no significant changes in psychometric slopes or in the performance on difficult or easy trials following CNO injection (**Figures 4G** to **4I**). Thus, consistent with the neuron-level effect of SOM interneuron activity on sensory processing in the local cortical circuits, SOM interneuron activity significantly contributed to perceptual discrimination of auditory stimuli at the behavioral level.

Discussions

To understand how behaviorally relevant computations are implemented in cortical circuits requires an appreciation of how distinct interneuron subtypes affect local networks during well-defined behavioral tasks. Earlier studies using *ex vivo* preparations revealed rich mechanisms for how different subtypes of interneurons affect local circuit properties (Cobb et al., 1995; Kapfer et al., 2007; Markram et al., 2004; Pfeffer et al., 2013; Silberberg and Markram, 2007; Xu et al., 2013). Recent years, with the availability of genetic targeting tools (Huang and Zeng, 2013; Luo et al., 2018) and cell-type specific recording and manipulation

methods (Fenno et al., 2011; Scanziani and Häusser, 2009), the functions of specific subtypes of inhibitory interneurons have been extensively investigated in intact mouse brain under anesthetized or quiet awake condition (Adesnik and Scanziani, 2010; Lakunina et al., 2020; Lee et al., 2012; Natan et al., 2017; Phillips and Hasenstaub, 2016; Schneider et al., 2014; Veit et al., 2017; Wilson et al., 2012). But to understand the impact of specific subtypes of inhibitory interneurons on cortical circuit computations, it is necessary to address this problem under well-defined behavioral tasks that make use of such computations and assess its contribution to behavioral functions (Kepecs and Fishell, 2014). Here we directly examined the functional role of SOM interneurons at both local circuit level and at behavioral level during a perceptual discrimination task. We found that SOM interneuron activity encodes both sensory stimuli and task-related categorical choice information (**Figure 1**), which emerged over learning (**Figure 2**). Using simultaneous optogenetic manipulation and two-photon imaging, we found that SOM interneuron activity exerts sharpening or scaling effect on the sensory representations of different groups of cortical neurons during task performance, with a greater proportion showing sharpened tuning by SOM interneurons (**Figure 3**). Consistent with the contribution of SOM interneurons to neuronal-level stimulus discrimination, inactivation of SOM interneurons specifically reduced the slope of psychometric functions that reflect perception-level sound discrimination (**Figure 4**). Our study provides evidence at both neuronal level and behavioral level supporting the direct contribution of SOM interneurons to cortical circuit computation underlying a perception function. This represents a new insight to the fundamental problem of how a major subtype of cortical interneuron contributes to circuit processing and behavioral functions.

Consistent with previous studies on sensory evoked responses in SOM interneurons (Lakunina et al., 2020; Li et al., 2014; Muñoz et al., 2017; Natan et al., 2017; Yu et al., 2019), we found that SOM interneurons in the auditory cortex show reliable responses to sound stimuli both during passive stimulation and task performance (**Figure 1**), with apparently longer response onset than other types of cortical neurons (**Figures 1** and **3**). This is consistent with the idea that SOM interneurons in sensory cortex receive majority of inputs from cortical feedback connections but not directly from ascending thalamic projections (Li et al., 2014; Yu et al., 2019). Intriguingly, we also observed a task-dependent enhancement of

210 SOM responses (**Figure 1D**), reflecting potential top-down modulation from higher order
211 areas (Liu et al., 2020) or from neuromodulatory input (Chen et al., 2015).
212 When targeting excitatory neurons, SOM interneurons mainly innervate apical dendrites
213 of cortical pyramidal neurons, exerting more specific control over synaptic integration that
214 can be distinct from the direct inhibition of spiking output by PV interneurons targeting
215 perisomatic domains. Moreover, SOM interneurons also target other subtypes of
216 interneurons, including both PV and VIP interneurons. Therefore, rather than mediating
217 conventional feedforward (Lakunina et al., 2020; Li et al., 2014) or feedback inhibition
218 (Silberberg and Markram, 2007), SOM interneurons may serve as a versatile regulator in
219 local cortical circuits, controlling the integration of top-down behavioral state information
220 and bottom-up sensory input during active perceptual behavior. Such uniqueness of SOM
221 interneurons warrant a dedicated investigation of its contributions to circuit and behavioral
222 functions, instead of as a comparison to other types of interneurons.
223 Using simultaneous two-photon population imaging and cell-type specific optogenetic
224 inactivation, we assess how SOM interneurons contribute to cortical circuit computations
225 during a behavioral task that specifically uses such computations. Our results show that SOM
226 interneurons either sharpen auditory frequency tuning or scale down the tuning peak of
227 different groups of local cortical neurons (**Figure 3**). A previous study in auditory cortex in
228 anesthetized mice also found similarly divergent effects on sensory tuning following SOM
229 inactivation, depending on different adaptation levels, with a sharpening the tuning for non-
230 adapted responses but a stronger scaling down effect for adapted responses (Natan et al.,
231 2017). This may, to some degree, correspond to the two types of modulations found in our
232 study, while the sharpening effect is also consistent with another recent study using quiet
233 awake mice (Lakunina et al., 2020). More importantly, here we were able to examine the
234 relationship between the SOM modulation effects and sensory discrimination during
235 behavior. We found that neurons with tuning curve sharpened by SOM neurons also
236 exhibited significant decrease in the discrimination of more similar stimulus (**Figure 3I**),
237 suggesting a contribution of SOM neurons to finer scale frequency discrimination. Since our
238 study did not use repeated stimulus to produce response adaptation, and hence we only find
239 the scaling effect in a minor proportion of neurons during behavior, which did not

240 significantly influence stimulus discrimination (**Figure 3J**). Consistent with the enhanced
241 neuronal level discrimination by SOM interneurons, at the behavioral level, inactivation of
242 SOM interneurons specifically reduced the slopes of the psychometric functions, influencing
243 discrimination of nearby but not far-away frequencies (**Figure 4**), providing a direct evidence
244 for the contribution of SOM interneurons to perceptual discrimination.

245 Here we examine the contribution of SOM interneurons using optogenetic inactivation
246 rather than activation. Previous studies mostly used activation of interneuron subtypes, and
247 showed diverse and even controversial effects (Atallah et al., 2012; Lee et al., 2012; Seybold
248 et al., 2015; Wilson et al., 2012), presumably due to different network states across
249 experiments (Seybold et al., 2015). It should also be noted that direct activation does not
250 represent physiological activity patterns, whereas inactivation manipulation is more proper
251 for examining the contribution of endogenous neuronal activity. Indeed, using inactivation
252 we observed specific impairment of perceptual function in finer-scale frequency
253 discrimination rather than general reduction in behavioral performance (**Figure 4**). Such
254 specific behavioral effect is in theory attributable to the neuronal level sharpening effect, also
255 revealed by SOM neuron inactivation (**Figure 3**).

256 Although SOM interneurons were modulated by choice behavior, the choice information
257 encoded in SOM interneurons may not directly be transmitted to local populations, since
258 photoinhibition of SOM interneurons did not significantly affect the choice coding of local
259 cortical neurons (**Figure S4**). The choice information in auditory cortical neurons is more
260 likely to be originated from higher order cortical regions (Liu et al., 2021; Zhong et al.,
261 2019).

262 In our current study, we primarily focused on SOM interneurons in the L2/3 of the
263 sensory cortex. The further diversity within SOM neurons and the differential functions of
264 SOM neurons in different cortical regions can be important directions for future studies, as
265 has been exemplified previously (Kvitsiani et al., 2013). Finally, since SOM interneurons
266 preferentially target distal dendrites of cortical principal neurons, how SOM interneurons
267 regulate dendritic integration during well-defined behavior is another important future
268 direction in dissecting the cellular mechanisms of cortical circuit computations.

Acknowledgments: We thank J. Pan for technical support; L. Cui and Y. Liu for help in developing the behavioral task. L. Deng for help in histology and animal preparation; C. A. Duan for discussion on data analysis; Z.M. Ying for lab administration.

Funding: This work was supported by the National Science and Technology Innovation 2030 Major Program (No. 2021ZD0203700 / 2021ZD0203704); National Key R&D Program of China (grant No. 2021YFA1101804); Lingang Lab (Grant No. LG2021XX-XX-XX LG202104-01-05); the NSFC-ISF International Collaboration Research Project, Grant No. 31861143034; the "Strategic Priority Research Program" of the Chinese Academy of Sciences, Grant No. XDB32010000 and XDA27010000; National Science Foundation for Distinguished Young Scholars (to N.L.X.).

Author contributions: R.C. and N.L.X. conceived the project and designed the experiments. R.C. performed the experiments and data analysis. Y.Z. performed the chemogenetic, experiments. R.C. and N.L.X. wrote the manuscript.

Competing interests: Authors declare no competing interests.

Data and materials availability: All data is available in the main text or the supplementary materials. All the original behavioral, optogenetic, chemogenetic, electrophysiological, imaging and tracing data and analysis code are archived in the Institute of Neuroscience, Chinese Academy of Sciences, and can be obtained upon reasonable request via email to the correspondence authors.

Methods

Mice

Experimental procedures were approved by the Animal Care and Use Committee of the CAS Center for Excellence in Brain Science and Intelligence Technology, Chinese Academy of Sciences. SOM-IRES-Cre mice were acquired from Jackson lab (Jax number: 013044). Animal age was 8-9 weeks at surgery, and age 9–10 weeks at the start of behavioral training. Mice were group-housed (< 6 mice/cage) in a 12 h reverse light/dark cycle. All experimental procedures were conducted during the dark phase. Mice had no previous history of any other experiments. Mice were water restricted before the start of behavioral training. Each mouse was weighted daily and the body weight was maintained at no less than 85% of the weight before water restriction. On training days, mice received all their water from behavioral task (~1 ml). Supplementary water was provided for mice who could not maintain a stable body weight from task-related water intake. On days without behavioral training, mice received 1 ml of water.

Surgery and virus injection

During surgery and virus injection, mice were anaesthetized with isoflurane (1~2%). For chronic imaging window implantation, a craniotomy of ~2 mm in diameter was made over the left auditory cortex, with the dura intact. The injection system is as described previously (Xin et al., 2019). A pulled glass pipette (25–30 um O.D. at the tip; Drummond Scientific, Wiretrol II Capillary Microdispenser) was filled with mineral oil, and positioned by a Sutter MP-225 manipulator. A metal plunger was inserted into pipette and controlled by a hydraulic manipulator (Narashige, MO-10) to load and inject viral solutions. For SOM neurons imaging, AAV-hSyn-FLEX-GCaMP6s (Shanghai Taitool Bioscience Co.Ltd) was slowly injected into left auditory cortex of SOM-IRES-Cre mice (10nl~20nl per minute, 100-150nl per site, 2-3 injection sites per animal). The imaging window is a double-layered glass window (inner layer, 200-um-thick, 2mm in diameter; outer layer, 220-um-thick, 5mm in diameter) adhered using an ultraviolet cured optical adhesive (Norland Optical Adhesives 61). The double-layered glass window was sealed with dental cement (Jet Repair Acrylic, Lang Dental Manufacturing), with the inner layer glass inserted in the craniotomy and outer

layer glass anchored on the skull. A titanium head-post was then attached to the skull using cyanoacrylate glue and dental cement. Mice were allowed for at least 7 days to recover before water restriction.

Head-fixed auditory discrimination behavior

The behavioral apparatus is as described previously (Xin et al., 2019; Zhong et al., 2019). Mice were head-fixed and placed in a custom-made double-walled sound-proof box. Mice were head-fixed, with water reward provided by two custom-made metal water spouts placed in front of the mice. The spouts are connected to a capacitive-sensing board that detect the contact of the tongue during licking. Mouse behavior was controlled by the PX-Behavior, a custom-developed real-time system, with the hardware controlled by a microcontroller (Arduino MEGA 2560) and software controlling task protocol and data acquisition written in C++ and python. Sound waveforms were generated from a custom-designed tone-generating module (TGM), sent to an amplifier (ZB1PS, Tucker-Davis Technologies), and delivered through electrostatic speakers (ES1, Tucker-Davis Technologies) placed on the right side of mice. The sound systems were calibrated using a free-field microphone (Type 4939, Brüel and Kjær) over 3–60 kHz and showed a smooth spectrum (± 5 dB). 5 ms cosine ramps are applied to the rise and fall of all tones.

After water restriction for 3-5 days, during which ~0.5 ml water per day was provided, mice showed motivation to lick to the spouts to obtain water reward. Behavioral training was started with an initial shaping session, where water was delivered upon licking at either of the lick spouts, alternating every 3 trials. Mice learned to lick left and right in this shaping session. The two-alternative-forced-choice (2AFC) task training was started 2-3 days after initial shaping. In the initial 2AFC task training, mice learned to discriminate two pure tones with 2 octaves apart (8 and 28 kHz, or 5 and 20 kHz). Mice were required to lick the left spout following the lower frequency tone and lick the right spout following the higher frequency tone. Each trial was started with a random delay of 500 ms to 2000 ms before sound stimulus onset. The sound stimulus lasts for 300 ms. The answer period (3 s) begins ~ 500 ms after the offset of sound stimulus. Mice were required to respond by licking within the answer period, during which licking on the correct side would lead to a water reward (~6

μl), while licking on the wrong side would lead to a time-out punishment of 2-4 s, during which continued licking on the wrong side would reinitiate the time-out period. If mice made no choice in the answer period, the trial was defined as a miss trial. The intertrial interval was 3 s between the end of the current trial and the start of the next trial. After mice learned the initial 2AFC task discriminating the two easy stimuli (reaching >85% correct rate), 4-6 additional tones at intermediate frequencies equally spaced in octaves between the two training tones were delivered to test the categorization performance and sensory tuning of imaged neurons. In the simultaneously manipulating SOM neurons and imaging experiment, besides the six frequencies with equal 0.4 octave distance, there was a tone of frequency at the defined boundary, randomly rewarded on both sides.

We fitted the behavior data with a sigmoid function to obtain the psychometric function of frequency discrimination (Carandini and Churchland, 2013; Wichmann and Hill, 2001; Xin et al., 2019)

$$y(x) = g + (1 - g - l) * 0.5 * (1 + \mathrm{erf}\,((x - u)/sqrt(2 * v\text{^}2)))$$

in which $y(x)$ represents the probability of rightward choice, x is octave distance of tone frequencies from the minimal frequency. The parameters: g is the guess rate, l is the lapse rate, u is subject bias, v is discrimination threshold (slope in our case). erf () is error function.

Two photon calcium imaging

We use a custom built two-photon microscope coupled to a Ti-Sapphire laser (Chameleon Ultra II, Coherent) to image the calcium signals in the auditory cortex. The laser was tuned to 920 nm. Signals were collected through a 16 x 0.8 NA objective (Nikon), isolated using a 594 nm high-pass dichroic and a bandpass filter (525/50, Semrock), and detected by GaAsP photomultiplier tubes (10770PB-40, Hamamatsu). Data were acquired using ScanImage at scanning rate of 55 Hz for 256×256 pixels, or 28 Hz for 512 × 512 pixels. The field of view is 447×447 μm for SOM neuron imaging, and 300×300 μm for pyramidal neuron imaging. At the beginning of each trial, the ScanImage receives a trigger from the behavior system to start data acquisition. Imaging experiments were conducted in a double-walled sound-proof

box enclosing the entire microscope to eliminate the ambient noise. The high frequency noise from the resonant scanner was blocked using a glass window sealing the metal housing of the scanner. Calcium imaging under passive condition was carried out after mice finished the behavioral task and with the lick ports removed.

Chronic imaging during learning

For imaging experiment across learning process, the same field location was tracked back by the blood vessel shape and position. For the same field, ROI selection were the same across days. There were still some neurons with visible location changing in the focal plane, and could be manually corrected. The neurons which were not constantly confirmed to be in the focal plane were excluded in analysis. All tones of six frequencies were given to mice both in early training stage and expert stage.

Simultaneous optical inhibition and imaging

AAV-Syn-GCaMP6s and AAV-Syn-FLEX-Jaws-KGC-tdTomato-ER2 were mixed with the titer ratio 1:10, and injected in the auditory cortex of SOM-Cre mice to allow the expression of Jaws in SOM interneurons and GCaMP6s in general L2/3 cortical neurons. To inactivate SOM neurons, 635 nm laser light was delivered through the objective via a custom-designed light path with an extra dichroic mirror (FF705-Di01, Semrock) and a modified primary dichroic mirror (FF594-Di04, Semrock) before the entrance pupil of the objective to pass the 635-nm laser into the objective and reflect the GCaMP6s emission light to the detection arm. The 635 nm light coming out of the objective was ~1 mm in diameter at the focal plan, with the total power of ~15 mW. The red laser pulse covered 1.5 s after sound onset in photostimulation trials, which were randomly interleaved with control trials at about equal proportions.

Imaging data analysis

In initial imaging data analysis, brain motion correction and regions of interest (ROIs) extraction follow the previous study (Xin et al., 2019). For SOM neuron, the baseline fluorescence(F0) of each trial is calculated by averaging the raw fluorescence of the time

window before sound. Then ΔF/F0 was calculated as (F – F0)/F0×100%, used as normalized fluorescence change across trials. For pyramidal neurons, imaging was done with continuous scanning, without gap during intertrial interval. Slow calcium fluorescence changes were removed by determining the distribution of fluorescence values in a ~20 s interval around each sample time point and subtracting the 8th percentile value. For each ROI, ΔF/F0 (%) was calculated as (ΔF/F0)×100, where F0 is the index of the peak of the histogram of F.

For further analysis of the behavior evoked response and tuning curves in behavior and passive condition, we use the peak of smoothed activity (by every 5 frames) in a fixed time window after sound. The fixed time window is 1.5 s for SOM neurons, and 1 s for pyramidal neurons, since the onset of calcium signal is slower in SOM neurons. For SOM neurons, correct trials in task were used, and for sound-tuned pyramidal neurons, both correct and error trials were used, since there is a middle frequency which was not assigned to a fixed side and rewarded randomly on both sides.

In the simultaneously optical manipulation and imaging experiment, we sometime observed overall fluorescence increase due to the 635 nm red laser illumination. To remove this optical artifact, first, we divided the imaging field into 100 x 100 (for field of 256 pixels x 256 pixels), or 200 x 200 (for field of 512 pixels x 512 pixels) sections. For non-ROI region of each section, in each photostimulation or control trial, baseline fluorescence (averaged fluorescence before 635 nm laser onset) were subtracted from fluorescence after laser onset. Then the subtracted fluorescence was averaged for all photostimulation trials (denoted by FO_d) or control trials (denoted by FN_d) respectively, after aligned to laser onset time. Then the artifact amplitude of the corresponding section is calculated as FO_d-FN_d. For each optical trial of each neuron, fluorescence after 635 nm laser onset was subtracted point-to-point by FO_d-FN_d of the section in which the neuron is located.

To quantify the effect of optogenetic inactivation of SOM interneurons, we used two-way analysis of variance (ANOVA, using MATLAB function 'anovan', linear model), with optical manipulation and frequency as the two contributing factors, to test the significance of

each factor contributing to the activity after sound onset of each trial. For each neuron, if p value of the photostimulation factor is below 0.05, and in further multi comparison, p value of at least one frequency is below 0.05, this neuron is defined as significantly modulated by photoinactivation. Comparing the mean activity of all trials in control trials versus photostimulation trials determined the neuron to be significantly increased or decreased.

We defined responsive neurons in task using the following criteria. For the preferred tone frequency, at least 70% of trials showed responses after stimulus onset exceeding 2 standard deviation of the pre-stimulus activity (baseline). We then classified neuronal responses as sensory or choice selective among the responsive neurons. Choice selective neurons were classified based on 1) two-way ANOVA with frequency and choice as the two contributing factors with the significance level of 0.01 for choice, and 2) fitting the frequency-response relation to a sigmoid function,

$$SR(x) = b1 + \frac{b2}{1 + e^{-\frac{(x-b3)}{b4}}}$$

with the R square > 0.8. Other responsive neurons which do not fulfill these criteria are classified as sound-tuned neurons.

To characterize SOM-sharpened and SOM-scaled neuron, we calculated the activity difference of each frequency under photostimulation and control condition (D_{freq}). If at least one D_{freq} of frequencies excluding BF is greater than the D_{freq} of BF, then it indicates that SOM neuron exerts more inhibition on other frequency than on BF and we consider this neuron as a SOM-sharpened neuron. On the contrary, if the activity difference of BF is the largest, it indicates this neuron is inhibited by SOM in a divisive manner, thus characterized as a SOM-scaled neuron. Tuning of SOM-sharpened neurons under control and photostimulation conditions were then aligned to the best frequency (BF) of control conditions, and normalized by subtracting the activity of the minimal response in each corresponding condition, and divided by the difference of BF response and the minimal response. The normalized responses were fitted with a Gaussian function (**Figure 3F**). Activity of each frequency of SOM-scaled neurons in photostimulation and control

conditions are summarized by subtracting the activity of the minimal response in control condition, and divided by the difference of maximal response and the minimal response in control condition (**Figure 3G**).

Chemogenetics inhibition

AAV-hSyn-FLEX-hM4Di-mCherry was injected bilaterally to mice auditory cortex. Clozapine N-oxide (CNO, 2-3mg/Kg, in 0.1ml solution) was intraperitoneally (i.p.) injected prior to the experimental sessions. In control sessions, 0.1ml saline was injected. Saline sessions and CNO sessions were interleaved, for paired comparison. Six probe middle frequencies were inserted with the total fraction of 40% trials. To control for the effect of CNO injection only, we injected CNO in mice expressing tdTomator in SOM interneurons (using AAV-hSyn-FLEX-tdTomato-WPRE-bGHpA), and obtained behavioral data.

Histology

After imaging or manipulation experiments, mice were deeply anesthetized with Chloral hydrate, and perfused with saline and then 0.4% Paraformaldehyde, to get the fixed brain tissue. Brains were fixed with Paraformaldehyde overnight or longer, and then dehydrated with 30% sucrose for at least one day. Then we cut brain slices using a cryostats (Leica CM1950). Images were taken using Olympus VS120.

Statistics

All data are presented as mean ± SEM, unless mentioned otherwise. Statistics were done using MATLAB R2017a. Statistical significance was tested using paired-sample t test, two-way-ANOVA, Wilcoxon signed-rank test. (ns, $p > 0.05$, *$p < 0.05$, **$p < 0.01$, ***$p < 0.001$.)

References

Adesnik, H., and Scanziani, M. (2010). Lateral competition for cortical space by layer-specific horizontal circuits. Nature *464*, 1155–1160. https://doi.org/10.1038/nature08935.

Atallah, B.V., Bruns, W., Carandini, M., and Scanziani, M. (2012). Parvalbumin-Expressing Interneurons Linearly Transform Cortical Responses to Visual Stimuli. Neuron *73*, 159–170. https://doi.org/10.1016/j.neuron.2011.12.013.

Atallah, B.V., Scanziani, M., and Carandini, M. (2014). Atallah et al. reply. Nature *508*, E3–E3. https://doi.org/10.1038/nature13129.

Carandini, M., and Churchland, A.K. (2013). Probing perceptual decisions in rodents. Nat Neurosci *16*, 824–831. https://doi.org/10.1038/nn.3410.

Chen, G., Zhang, Y., Li, X., Zhao, X., Ye, Q., Lin, Y., Tao, H.W., Rasch, M.J., and Zhang, X. (2017). Distinct Inhibitory Circuits Orchestrate Cortical beta and gamma Band Oscillations. Neuron *96*, 1403-1418.e6. https://doi.org/10.1016/j.neuron.2017.11.033.

Chen, N., Sugihara, H., and Sur, M. (2015). An acetylcholine-activated microcircuit drives temporal dynamics of cortical activity. Nat Neurosci *advance online publication*. https://doi.org/10.1038/nn.4002.

Chiu, C.Q., Lur, G., Morse, T.M., Carnevale, N.T., Ellis-Davies, G., and Higley, M.J. (2013). Compartmentalization of GABAergic Inhibition by Dendritic Spines. Science *340*, 759–762. https://doi.org/10.1126/science.1234274.

Cobb, S.R., Buhl, E.H., Halasy, K., Paulsen, O., and Somogyi, P. (1995). Synchronization of neuronal activity in hippocampus by individual GABAergic interneurons. Nature *378*, 75–78. https://doi.org/10.1038/378075a0.

Cottam, J.C.H., Smith, S.L., and Häusser, M. (2013). Target-Specific Effects of Somatostatin-Expressing Interneurons on Neocortical Visual Processing. J Neurosci *33*, 19567–19578. https://doi.org/10.1523/JNEUROSCI.2624-13.2013.

El-Boustani, S. El-Boustani et al. reply. 4. .

El-Boustani, S., and Sur, M. (2014). Response-dependent dynamics of cell-specific inhibition in cortical networks in vivo. Nat Commun *5*, 5689. https://doi.org/10.1038/ncomms6689.

Fenno, L., Yizhar, O., and Deisseroth, K. (2011). The Development and Application of Optogenetics. Annual Review of Neuroscience *34*, 389–412. https://doi.org/10.1146/annurev-neuro-061010-113817.

Fishell, G., and Rudy, B. (2011). Mechanisms of Inhibition within the Telencephalon: “Where the Wild Things Are.” Annu. Rev. Neurosci. *34*, 535–567. https://doi.org/10.1146/annurev-neuro-061010-113717.

Fu, Y., Tucciarone, J.M., Espinosa, J.S., Sheng, N., Darcy, D.P., Nicoll, R.A., Huang, Z.J., and Stryker, M.P. (2014). A Cortical Circuit for Gain Control by Behavioral State. Cell *156*, 1139–1152. https://doi.org/10.1016/j.cell.2014.01.050.

Huang, Z.J., and Zeng, H. (2013). Genetic Approaches to Neural Circuits in the Mouse. Annu. Rev. Neurosci. *36*, 183–215. https://doi.org/10.1146/annurev-neuro-062012-170307.

Iaccarino, H.F., Singer, A.C., Martorell, A.J., Rudenko, A., Gao, F., Gillingham, T.Z., Mathys, H., Seo, J., Kritskiy, O., Abdurrob, F., et al. (2016). Gamma frequency entrainment attenuates amyloid load and modifies microglia. Nature *540*, 230–235. https://doi.org/10.1038/nature20587.

Kapfer, C., Glickfeld, L.L., Atallah, B.V., and Scanziani, M. (2007). Supralinear increase of recurrent inhibition during sparse activity in the somatosensory cortex. Nat Neurosci *10*, 743–753. https://doi.org/10.1038/nn1909.

Kato, H.K., Gillet, S.N., and Isaacson, J.S. (2015). Flexible Sensory Representations in Auditory Cortex Driven by Behavioral Relevance. Neuron *88*, 1027–1039. https://doi.org/10.1016/j.neuron.2015.10.024.

Kepecs, A., and Fishell, G. (2014). Interneuron cell types are fit to function. Nature *505*, 318–326. https://doi.org/10.1038/nature12983.

Khan, A.G., Poort, J., Chadwick, A., Blot, A., Sahani, M., Mrsic-Flogel, T.D., and Hofer, S.B. (2018). Distinct learning-induced changes in stimulus selectivity and interactions of GABAergic interneuron classes in visual cortex. Nature Neuroscience *21*, 851–859. https://doi.org/10.1038/s41593-018-0143-z.

Kuchibhotla, K.V., Gill, J.V., Lindsay, G.W., Papadoyannis, E.S., Field, R.E., Hindmarsh Sten, T.A., Miller, K.D., and Froemke, R.C. (2017). Parallel processing by cortical inhibition enables context-dependent behavior. Nat Neurosci *20*, 62–71. https://doi.org/10.1038/nn.4436.

Kvitsiani, D., Ranade, S., Hangya, B., Taniguchi, H., Huang, J.Z., and Kepecs, A. (2013). Distinct behavioural and network correlates of two interneuron types in prefrontal cortex. Nature *498*, 363–366. https://doi.org/10.1038/nature12176.

Lakunina, A.A., Nardoci, M.B., Ahmadian, Y., and Jaramillo, S. (2020). Somatostatin-Expressing Interneurons in the Auditory Cortex Mediate Sustained Suppression by Spectral Surround. J. Neurosci. *40*, 3564–3575. https://doi.org/10.1523/JNEUROSCI.1735-19.2020.

Lee, S.-H. Interneuron subtypes and orientation tuning. 4. .

Lee, S., Kruglikov, I., Huang, Z.J., Fishell, G., and Rudy, B. (2013). A disinhibitory circuit mediates motor integration in the somatosensory cortex. Nat Neurosci *16*, 1662–1670. https://doi.org/10.1038/nn.3544.

Lee, S.-H., Kwan, A.C., Zhang, S., Phoumthipphavong, V., Flannery, J.G., Masmanidis, S.C., Taniguchi, H., Huang, Z.J., Zhang, F., Boyden, E.S., et al. (2012). Activation of specific interneurons improves V1 feature selectivity and visual perception. Nature *488*, 379–383. https://doi.org/10.1038/nature11312.

Letzkus, J.J., Wolff, S.B.E., Meyer, E.M.M., Tovote, P., Courtin, J., Herry, C., and Lüthi, A. (2011). A disinhibitory microcircuit for associative fear learning in the auditory cortex. Nature *480*, 331–335. https://doi.org/10.1038/nature10674.

Li, L., Ji, X., Liang, F., Li, Y., Xiao, Z., Tao, H.W., and Zhang, L.I. (2014). A Feedforward Inhibitory Circuit Mediates Lateral Refinement of Sensory Representation in Upper Layer 2/3 of Mouse Primary Auditory Cortex. J. Neurosci. *34*, 13670–13683. https://doi.org/10.1523/JNEUROSCI.1516-14.2014.

Liu, D., Deng, J., Zhang, Z., Zhang, Z.-Y., Sun, Y.-G., Yang, T., and Yao, H. (2020). Orbitofrontal control of visual cortex gain promotes visual associative learning. Nat Commun *11*, 2784. https://doi.org/10.1038/s41467-020-16609-7.

Liu, Y., Xin, Y., and Xu, N. (2021). A cortical circuit mechanism for structural knowledge-based flexible sensorimotor decision-making. Neuron *109*, 2009-2024.e6. https://doi.org/10.1016/j.neuron.2021.04.014.

Luo, L., Callaway, E.M., and Svoboda, K. (2018). Genetic Dissection of Neural Circuits: A Decade of Progress. Neuron *98*, 256–281. https://doi.org/10.1016/j.neuron.2018.03.040.

Markram, H., Toledo-Rodriguez, M., Wang, Y., Gupta, A., Silberberg, G., and Wu, C. (2004). Interneurons of the neocortical inhibitory system. Nature Reviews Neuroscience *5*, 793–807. https://doi.org/10.1038/nrn1519.

Muñoz, W., Tremblay, R., Levenstein, D., and Rudy, B. (2017). Layer-specific modulation of neocortical dendritic inhibition during active wakefulness. Science *355*, 954–959. https://doi.org/10.1126/science.aag2599.

Murayama, M., Pérez-Garci, E., Nevian, T., Bock, T., Senn, W., and Larkum, M.E. (2009). Dendritic encoding of sensory stimuli controlled by deep cortical interneurons. Nature *457*, 1137–1141. https://doi.org/10.1038/nature07663.

Natan, R.G., Rao, W., and Geffen, M.N. (2017). Cortical Interneurons Differentially Shape Frequency Tuning following Adaptation. Cell Reports *21*, 878–890. https://doi.org/10.1016/j.celrep.2017.10.012.

Pakan, J.M., Lowe, S.C., Dylda, E., Keemink, S.W., Currie, S.P., Coutts, C.A., and Rochefort, N.L. (2016). Behavioral-state modulation of inhibition is context-dependent and cell type specific in mouse visual cortex. ELife *5*, e14985. https://doi.org/10.7554/eLife.14985.

Pfeffer, C.K., Xue, M., He, M., Huang, Z.J., and Scanziani, M. (2013). Inhibition of inhibition in visual cortex: the logic of connections between molecularly distinct interneurons. Nat Neurosci *16*, 1068–1076. https://doi.org/10.1038/nn.3446.

Phillips, E.A., and Hasenstaub, A.R. (2016). Asymmetric effects of activating and inactivating cortical interneurons. ELife *5*, e18383. https://doi.org/10.7554/eLife.18383.

Pi, H.-J., Hangya, B., Kvitsiani, D., Sanders, J.I., Huang, Z.J., and Kepecs, A. (2013). Cortical interneurons that specialize in disinhibitory control. Nature *503*, 521–524. https://doi.org/10.1038/nature12676.

Scanziani, M., and Häusser, M. (2009). Electrophysiology in the age of light. Nature *461*, 930–939. https://doi.org/10.1038/nature08540.

Schneider, D.M., Nelson, A., and Mooney, R. (2014). A synaptic and circuit basis for corollary discharge in the auditory cortex. Nature *513*, 189–194. https://doi.org/10.1038/nature13724.

Seybold, B.A., Phillips, E.A.K., Schreiner, C.E., and Hasenstaub, A.R. (2015). Inhibitory Actions Unified by Network Integration. Neuron *87*, 1181–1192. https://doi.org/10.1016/j.neuron.2015.09.013.

Silberberg, G., and Markram, H. (2007). Disynaptic inhibition between neocortical pyramidal cells mediated by Martinotti cells. Neuron *53*, 735–746. https://doi.org/10.1016/j.neuron.2007.02.012.

Sohal, V.S., Zhang, F., Yizhar, O., and Deisseroth, K. (2009). Parvalbumin neurons and gamma rhythms enhance cortical circuit performance. Nature *459*, 698–702. https://doi.org/10.1038/nature07991.

Tremblay, R., Lee, S., and Rudy, B. (2016). GABAergic Interneurons in the Neocortex: From Cellular Properties to Circuits. Neuron *91*, 260–292. https://doi.org/10.1016/j.neuron.2016.06.033.

Urban-Ciecko, J., and Barth, A.L. (2016). Somatostatin-expressing neurons in cortical networks. Nat Rev Neurosci *17*, 401–409. https://doi.org/10.1038/nrn.2016.53.

Veit, J., Hakim, R., Jadi, M.P., Sejnowski, T.J., and Adesnik, H. (2017). Cortical gamma band synchronization through somatostatin interneurons. Nature Neuroscience *20*, 951–959. https://doi.org/10.1038/nn.4562.

Wichmann, F.A., and Hill, N.J. (2001). The psychometric function: I. Fitting, sampling, and goodness of fit. Perception & Psychophysics *63*, 1293–1313. https://doi.org/10.3758/BF03194544.

Wilson, N.R., Runyan, C.A., Wang, F.L., and Sur, M. (2012). Division and subtraction by distinct cortical inhibitory networks in vivo. Nature *488*, 343–348. https://doi.org/10.1038/nature11347.

Xin, Y., Zhong, L., Zhang, Y., Zhou, T., Pan, J., and Xu, N. (2019). Sensory-to-Category Transformation via Dynamic Reorganization of Ensemble Structures in Mouse Auditory Cortex. Neuron *103*, 909-921.e6. https://doi.org/10.1016/j.neuron.2019.06.004.

Xu, H., Jeong, H.-Y., Tremblay, R., and Rudy, B. (2013). Neocortical Somatostatin-expressing GABAergic Interneurons Disinhibit the Thalamorecipient Layer 4. Neuron *77*, 155–167. https://doi.org/10.1016/j.neuron.2012.11.004.

Yizhar, O., Fenno, L.E., Prigge, M., Schneider, F., Davidson, T.J., O'Shea, D.J., Sohal, V.S., Goshen, I., Finkelstein, J., Paz, J.T., et al. (2011). Neocortical excitation/inhibition balance in information processing and social dysfunction. Nature *477*, 171–178. https://doi.org/10.1038/nature10360.

Yu, J., Hu, H., Agmon, A., and Svoboda, K. (2019). Recruitment of GABAergic Interneurons in the Barrel Cortex during Active Tactile Behavior. Neuron *104*, 412-427.e4. https://doi.org/10.1016/j.neuron.2019.07.027.

Zhong, L., Zhang, Y., Duan, C.A., Deng, J., Pan, J., and Xu, N. (2019). Causal contributions of parietal cortex to perceptual decision-making during stimulus categorization. Nature Neuroscience *22*, 963. https://doi.org/10.1038/s41593-019-0383-6.

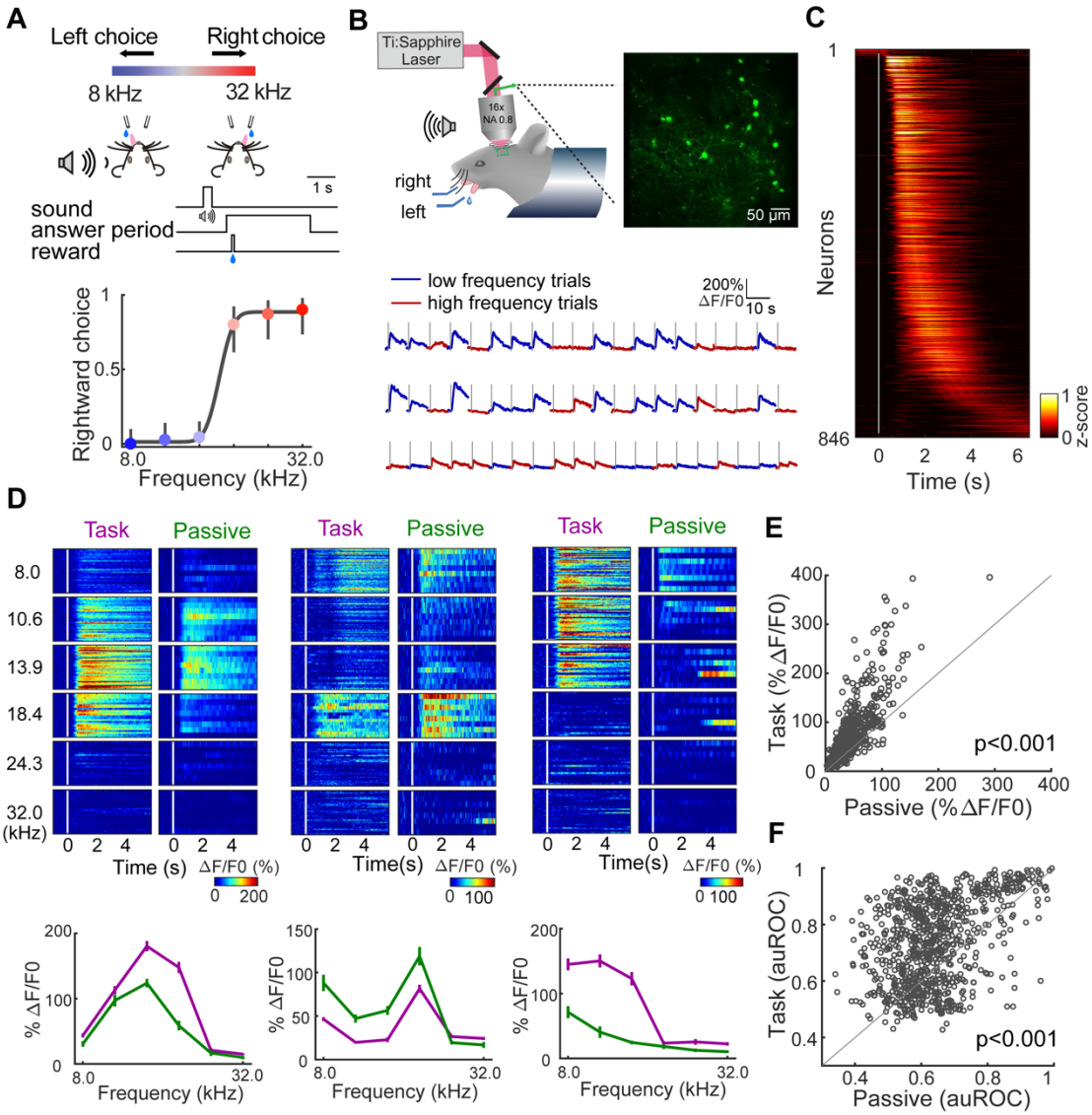

Figure 1. Two photon calcium imaging of SOM interneurons in auditory cortex in behaving mice

(A) Auditory frequency discrimination task. Top, schematic showing behavioral configuration. Bottom, psychometric curve of one example session. Error bar indicates 95% confidence interval.

(B) Two-photon calcium imaging from auditory cortical SOM interneurons in behaving mice. Upper, experiment configuration with an example imaging field showing GCaMP expressing SOM interneurons in auditory cortex. Bottom, calcium traces from three example SOM interneurons recorded during task performance.

(C) Calcium signals of all imaged SOM interneurons in task. Each row is z-scored calcium signals averaged across trials from one neuron. The white line is sound onset time.

(D) Activity in behaving and passive state from three example SOM interneurons. Left, a neuron showing stronger responses in task than in passive state. Middle, a neuron showing weaker responses in task than in passive state. Right, a neuron showing higher category discriminability in task than in passive state. Upper, color raster plot of calcium signals in individual trials grouped by tone frequency. Lower, mean response amplitude as a function of frequencies. Purple, task; green, passive. Calcium signals are all aligned to sound onset time, indicated by the white vertical lines. Error bars indicate SEM.

(E) Comparison of response amplitude in task and passive states for all imaged SOM interneurons. Each circle is the mean response amplitude from a single neuron ($P = 10^{-70}$, paired *t*-test, n = 846 neurons).

(F) Comparison of category discrimination (ROC analysis) in task and passive state. Each circle is a neuron ($P = 5.88 \times 10^{-63}$, paired *t*-test, n = 846 neurons).

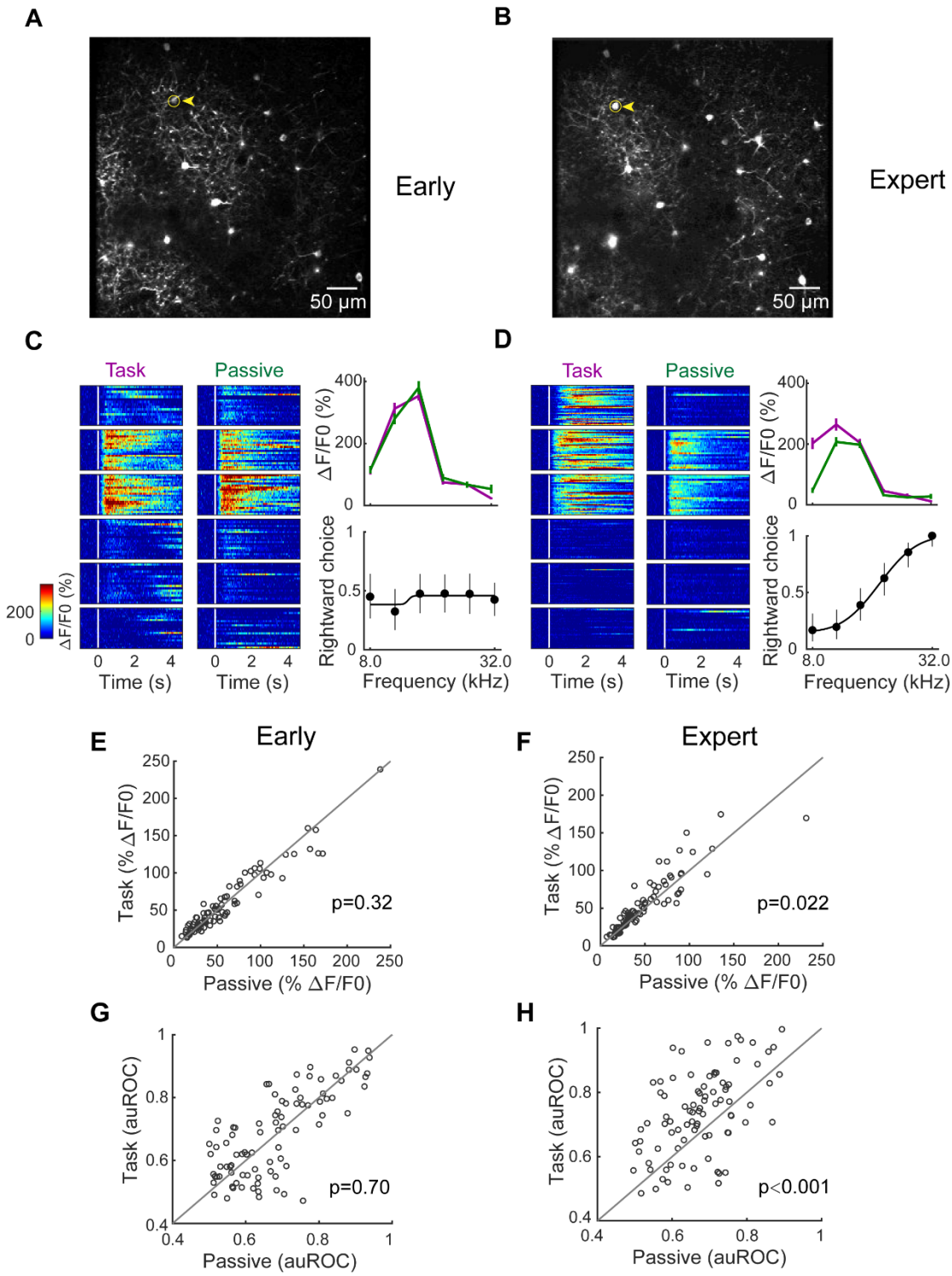

Figure 2. Task modulation of SOM interneurons is formed during learning
(A) and (B) Two-photon images of SOM interneurons from one example field in early and expert stage respectively. Yellow circle and triangle indicate the example neuron. (C) Activity of the example neuron indicated in (A) in task and passive states in early training stage. Behavioral performance is shown as the psychometric curve on the right. (D) As in (C) showing the activity from the same neuron and the behavioral performance in expert stage.

(E) Comparison of response amplitude of individual neurons under task and passive states in early training stage ($P = 0.32$, paired t-test; n = 88 neurons).
(F) Same as (E), but in expert learning stage ($P = 0.022$, paired t-test, n = 88 neurons).
(G) and (H) Comparison of category selectivity under task and passive conditions in early (G) and expert (H) learning stage respectively (paired t-test, n = 88 neurons).

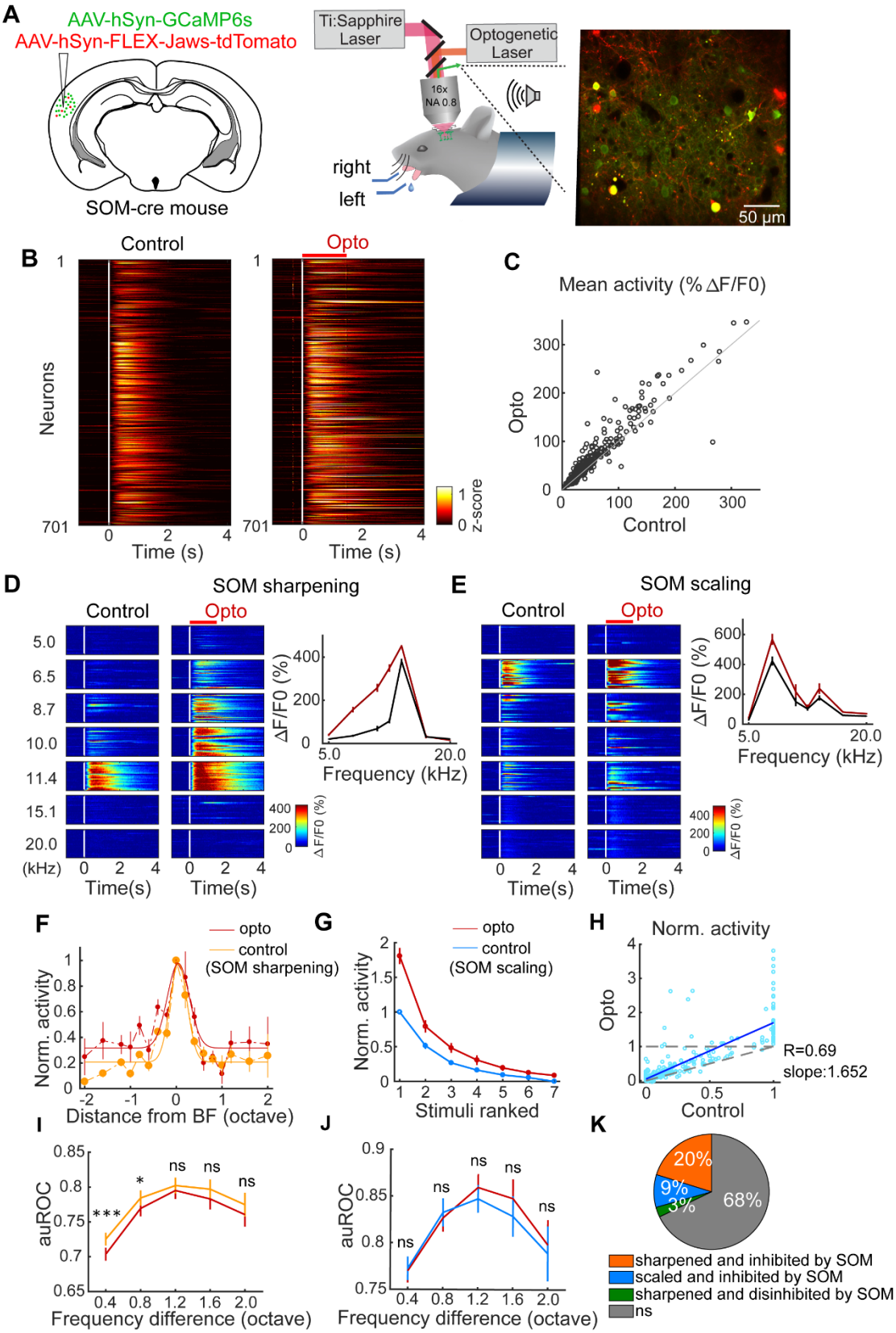
A
AAV-hSyn-GCaMP6s
AAV-hSyn-FLEX-Jaws-tdTomato
SOM-cre mouse
Ti:Sapphire Laser
Optogenetic Laser
16x NA 0.8
right
left
50 µm
B
Control
Opto
Neurons
Time (s)
z-score
C
Mean activity (% ΔF/F0)
Opto
Control
D
SOM sharpening
Control
Opto
(kHz)
Time(s)
ΔF/F0 (%)
Frequency (kHz)
E
SOM scaling
Control
Opto
Time(s)
ΔF/F0 (%)
Frequency (kHz)
F
opto
control
(SOM sharpening)
Norm. activity
Distance from BF (octave)
G
opto
control
(SOM scaling)
Norm. activity
Stimuli ranked
H
Norm. activity
Opto
Control
R=0.69
slope:1.652
I
auROC
Frequency difference (octave)
J
auROC
Frequency difference (octave)
K
20%
9%
3%
68%
sharpened and inhibited by SOM
scaled and inhibited by SOM
sharpened and disinhibited by SOM
ns

Figure 3. Inhibition of SOM interneurons reduced frequency discriminability of auditory neurons

(A) Schematic showing the virus injection (left) and simultaneous two-photon calcium imaging of auditory cortical neurons and optogenetic manipulation of SOM interneurons (right). Inset: one example imaging field. Green, neurons expressing GCaMP6s; red, SOM interneurons expressing Jaws; yellow, SOM interneurons expressing both GCaMP6s and Jaws.

(B) Calcium signals of all imaged putative non-SOM neurons in task with (left) or without (right) photostimulation. Each row is z-scored calcium signals averaged across trials from one neuron. The white vertical line is sound onset time. Red horizontal line indicates photostimulation time.

(C) Comparison of response amplitude in control and photostimulation conditions for all imaged putative non-SOM neurons. Each circle is the mean response amplitude from a single neuron.

(D) Activity of an example neuron sharpened by SOM interneurons. Left, color raster plot of calcium signals in individual trials grouped by tone frequency, with or without photoinhibition of SOM interneurons. Right, tuning curves in control and photostimulation conditions. Black, control condition; red, photostimulation condition.

(E) Same as (D), for an example neuron exhibiting scaling effect by SOM interneurons.

(F) Normalized activity of all SOM-sharpening neurons (including neurons inhibited and disinhibited by SOM neurons), as a function of tone frequency offset to the best frequency (BF) for each neuron. Orange, control condition; red, photostimulation condition. Error bars indicate SEM (n = 98 neurons).

(G) Normalized activity of each frequency of all SOM-scaling neurons, ranked by frequency preference and then averaged across neurons. Blue, control condition; red, photostimulation condition (n = 39 neurons).

(H) Comparison of normalized activity of each frequency for all SOM-scaling neurons under control and photostimulation conditions. Each dot represents the mean response to one frequency from one neuron. Dark blue line is the linear fitting result (n = 39 neurons).

(I) Discriminability for frequency pairs for each single SOM-sharpening neuron under control condition (orange) and photostimulation condition (red). Discriminability (auROC) is grouped and sorted by octave distance of each frequency pair, averaged across frequency pairs, and then averaged across neurons. Error bar indicates SEM (paired *t*-test, n = 98 neurons. ns, no significance; *, $P < 0.05$; ***, $P < 0.001$).

(J) Same as (I), but for SOM-scaling neurons.

(K) Fraction of each type of modulation by SOM interneurons.

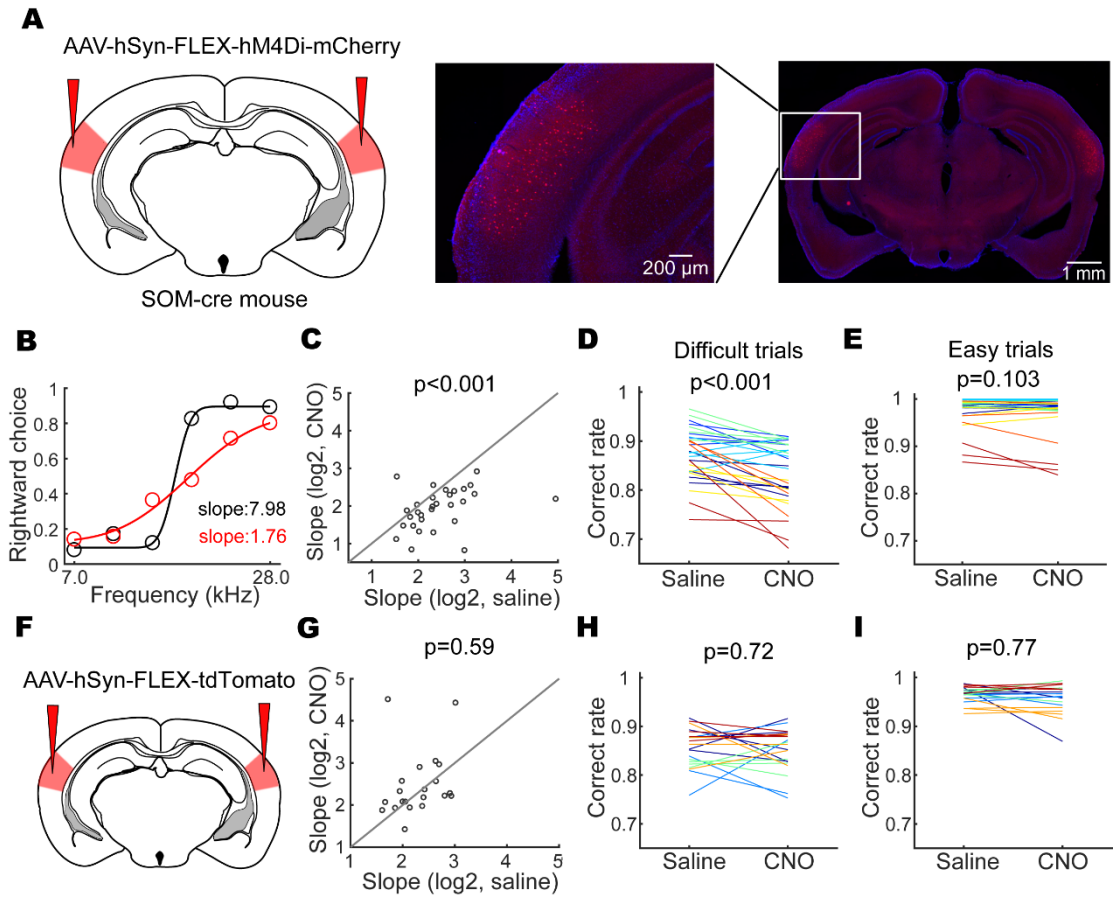

Figure 4. Inhibition of SOM interneurons impairs behavioral performance on perceptual discrimination

(A) Left, schematic showing the virus injection site expressing hM4Di in SOM interneurons. Right, histology imaging showing viral expression in auditory cortex.

(B) Psychometric functions showing behavior performance from a CNO injection session (red) and a saline injection session (control, black).

(C) Statistical comparison of psychometric function slope in saline and CNO sessions ($P = 6.89\times10^{-5}$, Wilcoxon signed-rank test, n = 30 session pairs from 7 mice, 3-5 session pairs from each mouse).

(D) Statistical comparison of correct rate of difficult trials (intermediate frequencies between 7 and 28 kHz) in saline and CNO sessions. Lines are data from alternating sessions with saline or CNO. Colors represents session pairs from different animals ($P = 8.19\times10^{-5}$, Wilcoxon signed-rank test, n = 30 session pairs from 7 mice).

(E) Same as (D), but for easy trials with end frequencies, 7 and 28 kHz ($P = 0.103$, Wilcoxon signed-rank test, n = 30 session pairs from 7 mice).

(F)-(I) Control experiments with tdTomato expressed in SOM interneurons in auditory cortex. Data presented as in (C)-(E) (Wilcoxon signed-rank test, n = 21 session pairs from 5 mice, 4 or 5 session pairs from each mouse).

Supplementary figures:

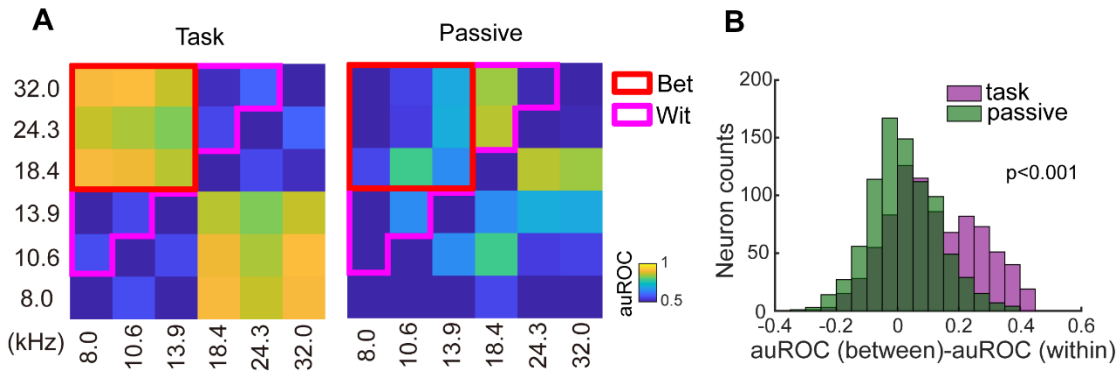

Figure S1. Pairwise discriminability of frequencies within or between categories
(A) Pairwise discriminability (auROC) of all frequencies from an example neuron, in task (left) and passive (right) state. Win, within the same (low or high) frequency category; Bet, between low and high frequency categories.
(B) In task, discriminability of frequencies from different categories is higher than that in the same category, and this difference is significantly larger than that in passive state (P=4.69×10^{-61}, paired t-test, n = 846 neurons).

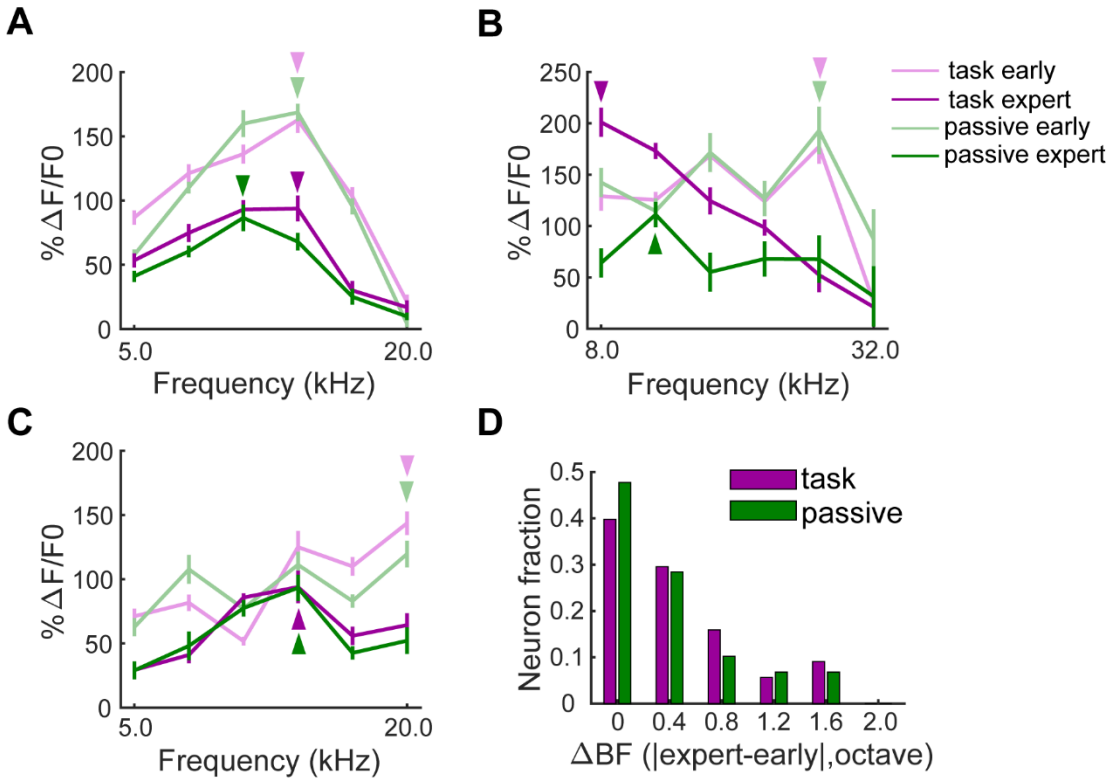

Figure S2. Sensory property of SOM neurons are largely maintained during learning.

(A)-(C) Tuning curves of three example neurons under task and passive state of different learning stage. Triangle indicates the position of BF.

(D) Summary of BF change across learning for all neurons, for task and passive state respectively.

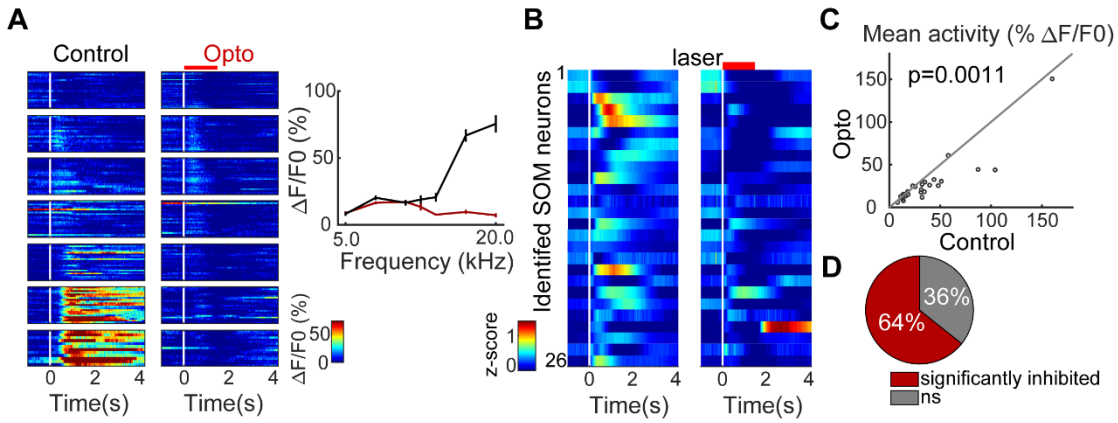

Figure S3. Efficiency of optogenetic manipulation on identified SOM neurons.
(A) Activity of one example identified SOM neuron co-expressing Jaws and GCaMP6s, under control and photostimulation conditions.
(B) Z-scored activity of all identified SOM neurons under control and photostimulation conditions. Each row is the z-scored activity averaged across all trials from one neuron.
(C) Comparison of response amplitude under control and photostimulation conditions for all identified SOM neurons. Each circle is the mean response amplitude in 1 s time window after sound, averaged across all trials from one neuron (P = 0.0011, paired t-test, n = 26 neurons).
(D) Quantification of activity change induced by photostimulation manipulation of all identified SOM neurons using ANOVA (n = 26 neurons).

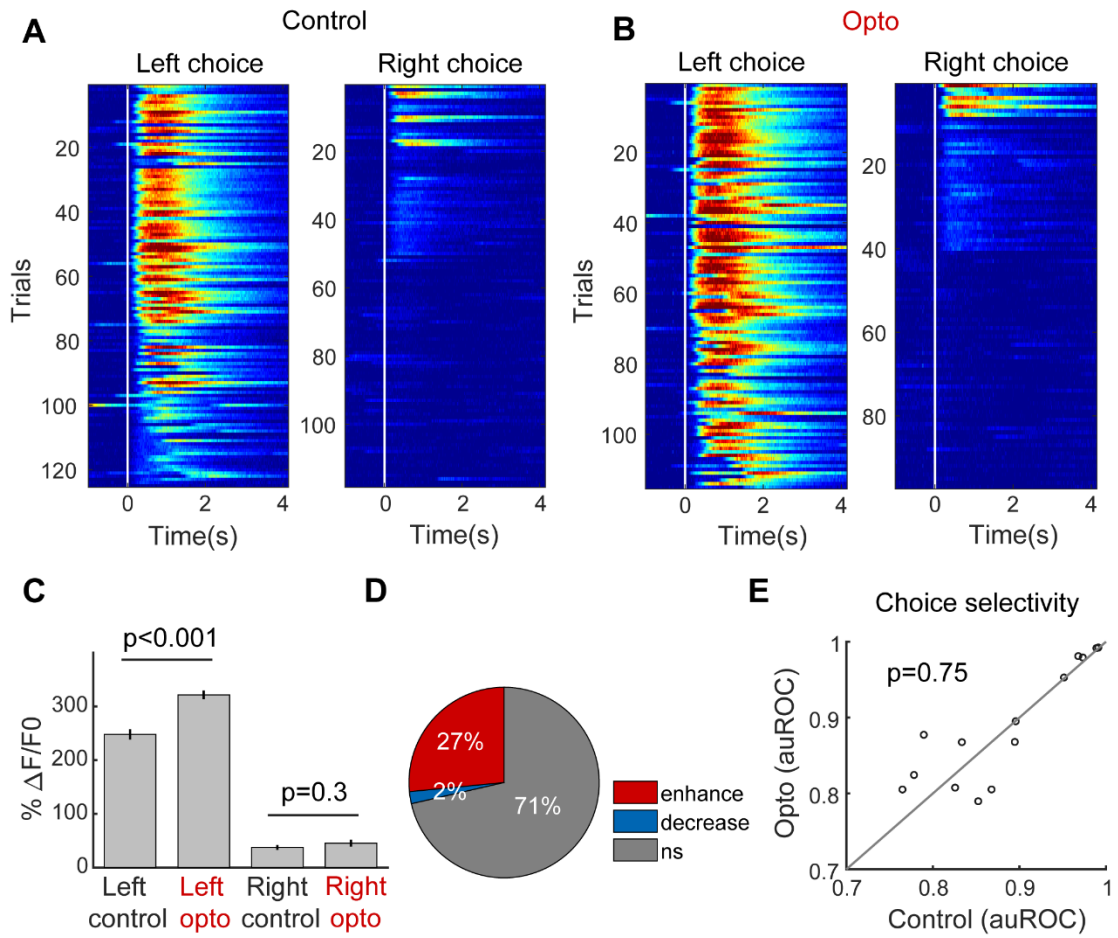

Figure S4. Effect of SOM neurons inactivation on choice selective neurons.
(A) Activity of one example choice selective neuron under control condition, showing different activity in trials choosing different side.
(B) Activity of the same neuron in (A), in photostimulation condition.
(C) Response amplitude averaged across trials for each condition in (A) and (B) (unpaired *t*-test).
(D) Quantification of activity change induced by photostimulation manipulation of all choice selective neurons using ANOVA (n = 49 neurons).
(E) Choice selectivity (ROC analysis) comparison of control and photostimulation conditions, for all choice selective neurons with significant activity amplitude change by photostimulation manipulation (paired *t*-test, n = 14 neurons).